Journal of
Marine Science and Engineering

MDPI

Article

Impact of Anthropogenic Climate Change on United States Major Hurricane Landfall Frequency

Emma L. Levin [1] and Hiroyuki Murakami [2,3,*]

1 Paul D. Schreiber High School, Port Washington, NY 11050, USA; emma.lilly10@yahoo.com
2 National Oceanic and Atmospheric Administration/Geophysical Fluid Dynamics Laboratory, Princeton, NJ 08540, USA
3 University Corporation for Atmospheric Research, Boulder, CO 80301, USA
* Correspondence: hir.murakami@gmail.com; Tel.: +1-609-452-5824

Received: 29 November 2018; Accepted: 6 May 2019; Published: 10 May 2019

Abstract: Although anthropogenic climate change has contributed to warmer ocean temperatures that are seemingly more favorable for Atlantic hurricane development, no major hurricanes made landfall in the United States between 2006 and 2016. The U.S., therefore, experienced a major hurricane landfall drought during those years. Using the high-resolution Geophysical Fluid Dynamics Laboratory 25 km grid High-Resolution Forecast-Oriented Low Ocean Resolution (HiFLOR) global climate model, the present study shows that increases in anthropogenic forcing, due to increases in greenhouse gasses, are associated with fewer long-duration major hurricane landfall droughts in the U.S., which implies an increase in major hurricane landfall frequency. We create six different fixed-distance 'buffers' that artificially circle the United States coastline in 100 km radial increments and can compensate for the bias in hurricane landfall calculations with six-hourly datasets. Major hurricane landfall frequencies are computed by applying the buffer zones to the six-hourly observed and simulated storm track datasets, which are then compared with the observed recorded major hurricane frequencies. We found that the major hurricane landfall frequencies generated with the 200 km buffer using the six-hourly observed best-track dataset are most correlated with the observed recorded major hurricane landfall frequencies. Using HiFLOR with an implemented buffer system, we found less frequent projections of long-duration major hurricane landfall drought events in controlled scenarios with greater anthropogenic global warming, which is independent on the radius of the coastal buffer. These results indicate an increase in U.S. major hurricane landfall frequencies with an increase in anthropogenic warming, which could pose a substantial threat to coastal communities in the U.S.

Keywords: major hurricane landfall drought; climate change and variability; climate modeling

1. Introduction

Notable for its high frequency of six major hurricanes (MHs), the 2017 Atlantic hurricane season resulted in severe damage in the United States and Caribbean [1]. Of the six MHs that formed in the North Atlantic, three made landfall in the North Atlantic. The two MHs that made landfall in the continental U.S. (Hurricanes Harvey and Irma) resulted in approximately $178.5 billion normalized economic damage [2,3]. Hurricane Harvey was the most devastating MH rainfall event ever recorded in U.S. history, with regions in eastern Texas experiencing over 60 inches of rainfall; Hurricane Irma was the strongest hurricane on record in the Atlantic Ocean Basin and cost the U.S. $51 billion [4–7]. Additionally in 2017, MH Maria devastated Puerto Rico, which resulted in approximately 5000 deaths and $90 billion damage [6,8]. Hurricane Harvey also terminated an 11-year 'drought' during which no MH had made landfall in the U.S. since Hurricane Wilma made landfall on 24 October 2005 [9,10].

This was the longest period without a MH landfall event since reliable record availability, and a recent study suggests that a drought of this duration is only expected to occur once every 400 years [11].

On the other hand, observed large-scale environmental factors had been favorable for tropical cyclone (TC) and MH activity over the tropical Atlantic during the drought period. Emanuel and Nolan [12] developed an empirical TC genesis potential index (GPI) and defined it as:

$$I = \left|10^5 \eta\right|^{\frac{3}{2}} \left(\frac{\mathcal{H}}{50}\right)^3 \left(\frac{V_{pot}}{70}\right)^3 (1 + 0.1 V_{shear})^{-2},$$

where η is the absolute vorticity in s^{-1}, $\mathcal{H}$ is the relative humidity at 700 hPa in percent, V_{pot} is the potential intensity in m s^{-1}, and V_{shear} is the magnitude of the vector shear from 850 to 200 hPa in m s^{-1}. This index can be a measure of favorable or unfavorable large-scale conditions for potential TC and MH genesis. The larger GPI anomalies over the tropical Atlantic during the MH landfall drought period (2006 to 2016) compared to the 1960s and 1970s reveal more favorable large-scale conditions for TC and MH genesis during the MH landfall drought period (Figure S1). Furthermore, globally seven of the ten warmest tropical sea surface temperature (SST) years on record took place during the 11-year MH landfall drought (from 2006 to 2016) [13]. These factors imply that during the MH landfall drought, atmospheric and oceanic conditions were more favorable for TC and MH occurrence than in previous decades [14–16]. Although the duration of this MH landfall drought is the longest on record, the drought event cannot be considered robust, as recorded drought duration is heavily dependent on the parameters used to define MH, such as maximum wind speed and minimal sea level pressure; by altering the variables used to define a MH landfall event, the recorded MH landfall frequencies will change [17].

Although a number of global climate models (GCMs) project a decrease in TC frequency in the North Atlantic, as well as the global domain in the future, a greater proportion of the TCs in this basin are predicted to be considered MH with a Saffir–Simpson Category 3 or higher rating [18–24], for which most of the conventional GCMs are unable to simulate due to their coarse horizontal resolution. Additionally, previous studies anticipate that with an increase in greenhouse gases in the atmosphere and an increase in global temperatures, mean TC tracks in the North Atlantic could shift eastward, leading to a decrease in the hurricane landfall frequencies in this basin [25–27]. We question whether the aforementioned recent lack of MH landfall activity in the North Atlantic (2006 to 2016) occurred due to anthropogenic global warming, intrinsic natural variability, or just occurred stochastically. We also seek to assess the projected frequencies of MH landfall events with changes in anthropogenic forcing.

Previous studies reported that the Geophysical Fluid Dynamics Laboratory (GFDL) High Resolution Forecast-oriented Low-ocean Resolution coupled model (HiFLOR) has skill in simulating and predicting MHs in the North Atlantic and is a sound tool for MH analysis [28–33]. In this paper, we utilize HiFLOR to investigate the projected change in U.S. MH landfall drought frequency with an increase in anthropogenic forcing. Section 2 describes our methods for determining predicted MH landfall drought occurrences with varying extensions of the U.S. coastline, and Section 3 describes our findings. We conclude, in Section 4, with a discussion of our work, future research and the implications of a projected decrease in long MH landfall droughts (an increase in MH landfall frequency) in the U.S.

2. Methods

2.1. Definition of Landfall and Observation Analysis

We seek to address potential biases in hurricane landfall frequencies derived from six-hourly datasets like the National Hurricane Center's HURDAT2 (http://www.aoml.noaa.gov/hrd/hurdat/Data_Storm.html [34]) dataset or GCM outputs. In contrast to the Hurricane Research Division's observed landfall frequencies (http://www.aoml.noaa.gov/hrd/hurdat/UShurrs_detailed.html [9]), which utilize the exact time and coordinate points of the storm's landfall position in the landfall frequency calculation, observed TC tracks and landfalls by HURDAT2 and simulated TC tracks and landfalls are detected

using six-hourly outputs. The six-hourly datasets do not account for any hurricane activity and track shifts in between the six-hourly checkpoints of the storm. The 6-hour lapse of time in between track nodes could lead to inaccuracies in hurricane landfall calculations because the timing of a storm crossing the coastline is not always detected in six-hourly time steps. Generally, TC intensity rapidly decreases after it makes landfall. Therefore, if we define MH landfall events only for TCs over a land surface with MH intensity at the time of a six-hourly node, we could overlook several MH landfall events. Because the six-hourly HURDAT2 dataset and GCM outputs continue to be utilized to analyze and predict catastrophic landfall activity, it is important that these mechanisms predict the most accurate frequencies as possible. This is especially true for MH landfall frequencies because of their destructive nature and the fact that mean MH landfall frequencies are typically low (<1.0) in the U.S. [8]. Therefore, we seek to create a new system that analyzes hurricane landfall activity that is suitable to adjust bias in six-hourly datasets. We also seek to use this system to understand the effects of anthropogenic forcing on MH landfall frequencies in response to the 11-year MH landfall drought.

We changed the parameters of a landfall event with the creation of a 'buffer' system. Using a Geographic Information System (GIS), QGIS, [35,36] we created 6 fixed-distance buffers that circled the U.S. eastern coastal state border line with six different radii in 100 km increments; 0 km, 100 km, 200 km, 300 km, 400 km, and 500 km (Figure 1). This created a closed loop around the eastern coast of the U.S., in both inward and outward directions. With each buffer, we defined a landfall event to occur when a TC center crosses the artificial buffer, rather than the true coastline. In doing so, we included in our statistics MHs that actually crossed coastlines with major hurricane intensity but were overlooked in six-hourly datasets. We utilized the shapefile representing the 2015 U.S. coastline for our analysis.

Given the fact that the observed mean radius at which the azimuthal-mean winds speed is 12 m s^{-1} (r_{12}) ranges between 125 km to 500 km for the TCs over the North Atlantic (Figure 4 in [37]), we stopped expanding the buffer distance at 500 km for our analysis. However, this expansion of buffer distance may also cause overestimation of MH landfall events provided that MHs were located within a buffer but do not cross a coastline. Even so, we accounted for intense storms located adjacent to the east coast of the U.S. that can cause severe damage to coastal communities, whether or not they were officially considered MH landfall events (indirect hits) [38]. On the other hand, a smaller buffer can also cause underestimation of MH landfall event counts. For example, when the 0 km buffer was used to define a MH landfall using the six-hourly HURDAT2 dataset, there was no MH landfall event detected for the year 2005 (Figure 1a), although there were a number of MHs that actually crossed U.S. coastline that year [9]. This was mainly because the observed MH landfalls were not detected in the six-hourly dataset. In this study, we not only seek to address MH landfall events, but potentially hazardous MHs near the coast of the United States and how they react to changes in anthropogenic forcing. Given the fact that mean storm size on average reaches up to 500 km in radius [37,39], taking a buffer could improve estimating storm risk over land and give us a larger sample size of storms near the coast of the United States that could be detrimental to coastal communities. Our final goal is to examine how the HiFLOR-generated MH landfall predictions change for each buffer with different levels of anthropogenic forcing. Although we defined MH landfall for the MHs within the buffer system for convenience, the frequency of MHs within the buffer system did not always match the actual MH landfall frequencies especially for a larger buffer size. Therefore, this study qualitatively analyzed the relationship between anthropogenic forcing and frequencies of MHs near the coastal United States. We seek to address if there were any discrepancies of the projected changes in MH landfall frequencies on the buffer size.

We obtained the 116-year North Atlantic TC track data for the period of 1900 to 2015 from the National Hurricane Center Data Base HURDAT2 (http://www.aoml.noaa.gov/hrd/data_sub/re_anal.html), which includes a six-hourly output of location, maximum surface wind speed, and central pressure [34]. We ran this observed track data through each artificial buffer and computed the seasonal MH landfall frequencies for each buffer according to our revised definition of landfall (e.g., Figure 1), which was then compared to recorded seasonal MH landfall frequencies from the Hurricane Research

Division (http://www.aoml.noaa.gov/hrd/hurdat/UShurrs_detailed.html) [9]. If a TC maintained at the threshold parameters of ≥50 m s^{-1} at the first output after which it has made landfall according to our buffer parameters, this event was considered as a MH landfall for our convenience. For this reason, the MH landfalls frequencies, determined with our six-hourly buffer system using HURDAT2 data, were not always the same as MH landfall frequencies calculated from the Hurricane Research Division (Figure 1).

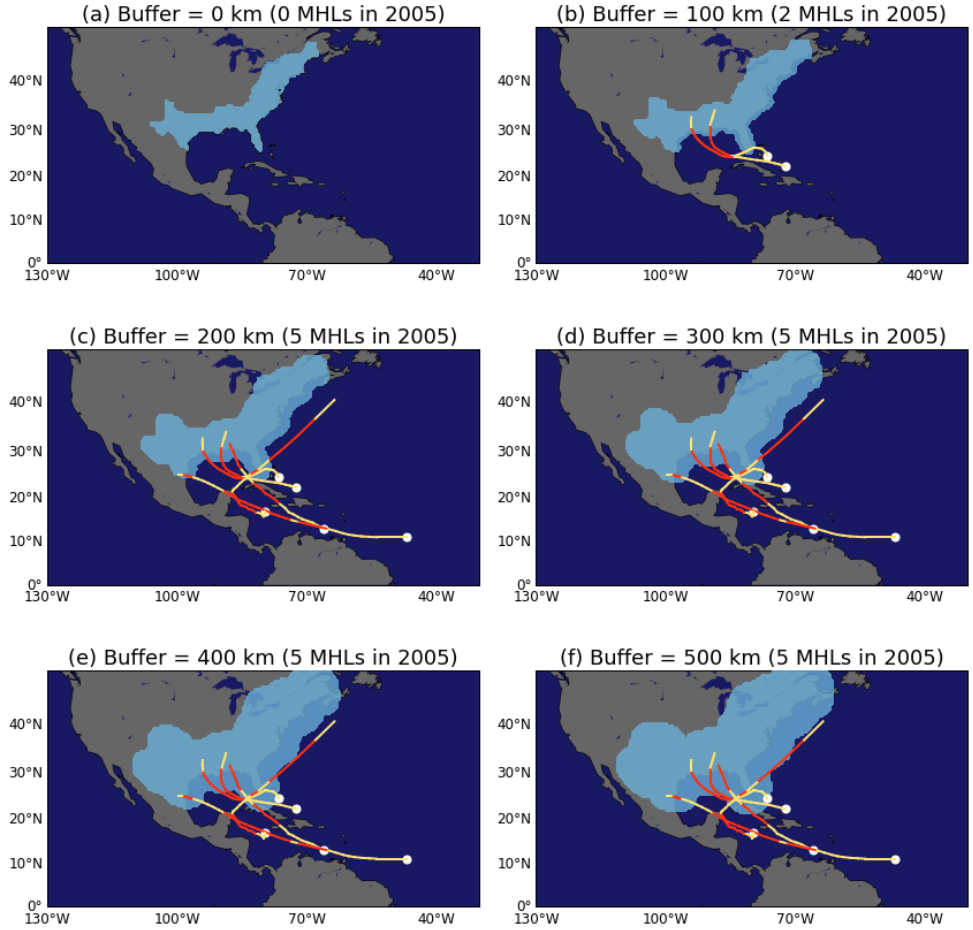

Figure 1. Fixed- distance artificial buffers applied at (**a**) 0 km, (**b**) 100 km, (**c**) 200 km, (**d**) 300 km, (**e**) 400 km, (**f**) 500 km from the true coastline. When a TC has crossed into the blue shading domain, it was considered to have made landfall. Plotted are major hurricane (MH) tracks in 2005 that fall into the buffer domains based on the HURDAT2 six-hourly dataset. Colors indicate storm intensity (red corresponds to MH intensity and yellow corresponds to storms weaker than major hurricane intensity). White dots indicate locations of storm genesis.

2.2. Model Simulations

In this study, we utilized HiFLOR, a high-resolution 25 km × 25 km mesh atmospheric/land and 100 km × 100 km ocean/sea-ice coupled global model. As stated by Murakami et al. (2015) [28], HiFLOR was created as an increased-resolution version of the Forecast-oriented Low Ocean Resolution model (FLOR, [13]), which consists of 25-km mesh atmospheric/land components from the GFDL Coupled Model, version 2.5 (CM2.5; [40]) and 1° ocean and sea ice components based on the GFDL Coupled Model, version 2.1 (CM2.1; [41]). Adjustments to the parameterization of ocean roughness in the FLOR model to create the HiFLOR model enabled it to simulate and predict TC events, especially intense MH events [28,30,42], with greater accuracy (Figures S2 and S3). To assess how well HiFLOR represented MH landfall frequencies, we used simulated TC track data detected by a TC tracking

scheme [28,43] for model simulations including location, maximum wind speed, and central pressure from six-hourly output from GFDL HiFLOR simulations. We used a 300-year climate simulation developed by Murakami et al., 2015 [28], that depicts the climate conditions characteristic of the year 1990 and maintains fixed forcing agents of atmospheric CO_2, CH_4, N_2O, halons, tropospheric and stratospheric O_3, anthropogenic tropospheric sulfates, black and organic carbon, and solar irradiance [28]. The same methods were used to create a 1200-year climate simulation that depicts climate conditions characteristic of the year 1860 as well as 200-year, 300-year, and 200-year simulations characteristic of the years 1940, 1990, and 2015, respectively. The 1860 and 1940 control simulations include lower SST in the North Atlantic, in comparison to the 1990 and 2015 control simulations because of the cooler climatic conditions of the mid-19th century and early 20th century. To eliminate climate drifts with the models in our analysis, we removed the first 50 years of each climate simulation to ensure stability. Therefore, we analyzed 1150 years of the 1860 control, 150 years of the 1940 control, 250 years of the 1990 control, and 150 years of the 2015 control.

Because each simulation ran for a different duration of time, for each control simulation we computed a 116-year moving mean frequency of cumulative MH landfall droughts stratified by duration. This was the length of the time frame for our 1900 to 2015 observational data, and we ensured consistency with our data timeframe for all experimental groups. A caveat with this approach was that, except for the 1860 climate simulation, the shorter 200 to 300-year simulations were not long enough to obtain enough samples for the 116-year moving mean average, especially with the removal of the first 50 years of the simulation in our analysis, leading to possible sampling errors in the statistics. We completed these calculations at each fixed-distance buffer. We computed these mean drought durations and frequencies with each simulation and observational data to accomplish three objectives:

1. Identify which buffer distance applied to the six-hourly HURDAT2 matches the observed recorded MH landfall frequency.
2. Compare the MH landfall frequencies of the 6-houly HURDAT2, early control simulations, and late control simulations for each buffer distance to assess how closely HiFLOR's MH landfall statistics match those in the observational data.
3. Compare the simulated frequencies of MH landfall drought events among the control simulations with different buffer distance to determine the effects of anthropogenic forcing on the length of MH landfall drought in the U.S., and to identify the dependency of the results on buffer distance.

3. Results

3.1. Sensitivity of Buffer Distance to United States MH Landfall Frequencies

Table 1 shows the mean annual observed frequency of landfall events with the buffer system using the six-hourly HURDAT2 dataset, the difference from recorded annual landfall frequency from National Oceanic and Atmospheric Administration (NOAA)'s Hurricane Research Division, and the correlation between the buffer and recorded landfall events for MHs as well as all storms (i.e., TC landfall). When the six-hourly HURDAT2 TC tracks in the North Atlantic from 1900 to 2015 were run through all six buffers, the mean TC landfall frequency for each buffer was at least one additional event than what was recorded by NOAA. As expected, (c) in Table 1 shows a positive correlation between TC landfall frequency and buffer distance. The yearly TC landfall frequencies for all buffers were positively and moderately correlated with the recorded data ($r > 0.60$). In contrast, with observed MH landfall frequencies, we found that the mean yearly frequencies recorded by NOAA were greater than the mean yearly frequencies computed with the HURDAT2 dataset using 0 km and 100 km buffers ((e) in Table 1). We also found that by running the HURDAT2 dataset through all other buffers, the number of MH landfall events was greater than the recorded data using the buffers larger than or equal to 200 km. (f) in Table 1 shows that yearly MH landfall frequencies with all buffers ≥ 100 km were highly correlated with the yearly recorded MH landfall frequencies ($r > +0.8$).

Table 1. (a) Mean annual TC landfall frequency with buffer (1900 to 2015) using the six-hourly HURDAT2 dataset, (b) the difference between mean annual TC landfall frequency with buffer and mean annual frequency of recorded TC landfall frequency from NOAA, and (c) the correlation between observed annual TCL frequencies with buffer and recorded TC landfall frequency from NOAA with *p*-value in parenthesis. (d) to (f) match measures of (a) to (c), except these measures were taken with MH landfall frequencies.

	TC Landfall			MH Landfall		
Buffer	**(a) Freq**	**(b) Diff**	**(c) Correl (*p*-Value)**	**(d) Freq**	**(e) Diff**	**(f) Correl (*p*-Value)**
0 km	2.76	+1.14	0.71 (2.00×10^{-16})	0.19	−0.42	0.33 (3.12×10^{-4})
100 km	3.37	+1.75	0.75 (2.20×10^{-16})	0.50	−0.11	0.80 (2.20×10^{-16})
200 km	3.97	+2.35	0.71 (2.20×10^{-16})	0.74	+0.13	0.86 (2.20×10^{-16})
300 km	4.40	+2.78	0.68 (2.20×10^{-16})	0.84	+0.22	0.86 (2.20×10^{-16})
400 km	4.92	+3.30	0.67 (2.48×10^{-16})	0.94	+0.33	0.84 (2.20×10^{-16})
500 km	5.39	+3.77	0.63 (5.22×10^{-14})	0.99	+0.38	0.84 (2.20×10^{-16})

Figure 2 demonstrates that by differing the buffer distance used to define MH landfall, the length of recent U.S. MH landfall drought changed drastically. The recorded MH landfall drought was 11 years in length during the period 2006 to 2015. However, with the use of a 0 km buffer, the drought was considered to have lasted for the period 1993 to 2015; while using the 500 km buffer we found that the longest drought between 1900 and 2015 would have lasted from 2011 through 2015 (Figure 2). In summary, we found that the 200 km buffer was the closest match to the recorded NOAA data in terms of both the mean and interannual variation of MH landfall frequency.

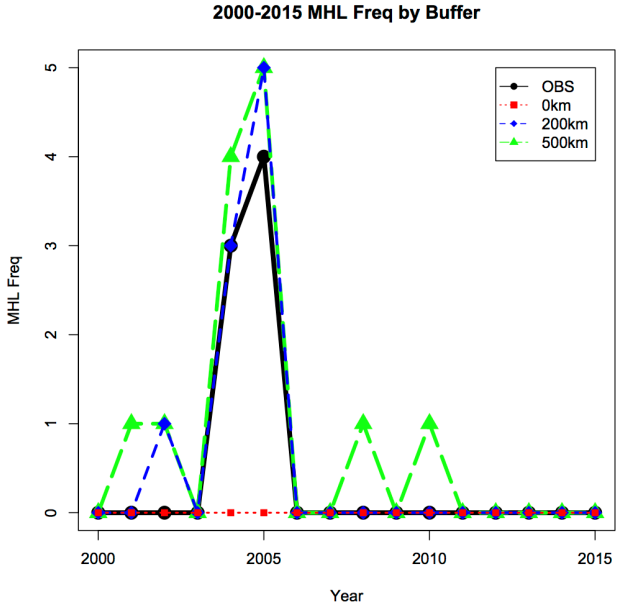

Figure 2. Recorded annual MH landfall frequencies from NOAA's Atlantic Hurricane Database (black), observed major hurricane landfall frequencies using six-hourly HURDAT2 with a 0 km fixed-distance buffer (red), 200 km fixed-distance buffer (blue), and 500 km fixed distance buffer (green) for the period 2000 to 2015.

By extending the buffer distance and accounting for a greater frequency of landfall events, the relationships between climate variables (MH landfall frequency, TC frequency, TC landfall frequency, mean summer Niño-3.4 index, and mean summer SST over the main development region form MHs (10–25° N and 20–80° W; [30]) became more highly correlated (Table 2). This higher correlation for

larger buffer distances was not surprising because a greater sample of MH landfall events was included in the larger buffer distances.

Table 2. Correlation coefficients between (a) observed annual MH landfall (MHL) frequency with buffer and annual TC landfall (TCL) frequency with buffer, (b) observed annual basin-total TC frequency over the North Atlantic (NA) and annual TCL frequency with buffer, (c) observed annual basin-total TC frequency over the NA and annual MHL frequency with buffer, (d) seasonal mean (July to October) Niño-3.4 Index and annual TC landfall frequency with buffer, (e) seasonal mean (July to October) El Niño 3.4 Index and annual MHL frequency with buffer, (f) seasonal mean (July to October) SST over the Main Development Region (MDR; 10–25° N, 20–80° W) and annual TC landfall frequency with buffer, and (g) seasonal mean (July to October) SST over MDR and annual MHL frequency with buffer. The analyzed period for the correlation coefficients is 1900 to 2015. *p*-values for significance testing are in parentheses.

Buffer (km)	(a) MHL and TCL	(b) TC and TCL	(c) TC and MHL	(d) Niño-3.4 and TCL	(e) Niño-3.4 and MHL	(f) MDR and TCL	(g) MDR and M. MHL
0	0.21 (*0.02*)	0.41 (5.31×10^{-6})	0.08 (0.38)	−0.29 (1.62×10^{-3})	−0.14 (0.12)	0.16 (0.09)	0.07 (0.42)
100	0.41 (*5.80* $\times 10^{-6}$)	0.45 (3.83×10^{-7})	0.16 (0.08)	−0.27 (3.10×10^{-3})	−0.20 (0.03)	0.17 (0.08)	0.09 (0.31)
200	0.47 (*1.43* $\times 10^{-7}$)	0.55 (1.67×10^{-10})	0.34 (1.60×10^{-4})	−0.33 (2.68×10^{-4})	−0.28 (2.06×10^{-3})	0.22 (0.02)	0.13 (0.17)
300	0.46 (*1.43* $\times 10^{-7}$)	0.60 (1.79×10^{-12})	0.34 (2.29×10^{-4})	−0.38 (2.94×10^{-5})	−0.33 (3.23×10^{-4})	0.24 (8.60×10^{-3})	0.14 (0.13)
400	0.53 (*1.27* $\times 10^{-9}$)	0.65 (4.10×10^{-15})	0.37 (4.88×10^{-5})	−0.40 (1.10×10^{-5})	−0.37 (5.09×10^{-5})	0.23 (0.01)	0.19 (0.04)
500	0.53 (*8.86* $\times 10^{-10}$)	0.69 (2.20×10^{-16})	0.37 (3.43×10^{-5})	−0.42 (2.93×10^{-6})	−0.37 (4.21×10^{-5})	0.26 (0.01)	0.20 (0.03)

3.2. Impact of Anthropogenic Climate Change on MH Landfall Drought

Figure 3a shows the simulated mean frequency of consecutive years, during which no MH made landfall (i.e., the duration of MH landfall drought). A 200-km buffer is used for the 116-year moving means of the HiFLOR 1860 control and the HiFLOR 1990 control. We depicted this buffer because the observed MH landfall frequencies detected using six-hourly HURDAT2 dataset with this buffer most closely match the observed recorded MH landfall frequencies in the United States than any other buffer as analyzed in Section 3.1. It is important to note that the horizontal axis in Figure 3 represents a minimum length of MH landfall drought; namely, '20' represents MH landfall drought length longer than or equal to 20 years. The 1990 control illustrates a greater frequency of droughts with shorter than 11 years in the minimum length, while the 1860 control illustrates a greater frequency of droughts with longer than 11 years in the minimum length. This indicates that HiFLOR projected a greater frequency of MH landfall events under conditions of higher anthropogenic forcing, as demonstrated by the higher (lower) frequency of shorter (longer) droughts for the 1990 control than the 1860 control. There was a small error bar that overlapped between the mean MH landfall drought frequencies of the 1860 control and the 1990 control for the shorter and longer drought durations, indicating the significance in the differences between calculated frequencies. These results were generally consistent for the other buffer distances, all of which demonstrated the 1990 control simulation to exhibit a greater frequency for shorter MH landfall droughts, while the 1860 control depicted a greater frequency for longer MH landfall droughts (Figure 3b,c).

The above conclusion was also reached when we compared the climate model simulations with different levels of anthropogenic forcing (Figure 4). Figure 4 displays mean MH landfall drought frequency simulated by a series of control experiments using the 200 km buffer, showing that simulated frequency of shorter (longer) MH landfall drought events was generally projected to increase (decrease) as the level of anthropogenic forcing increased, which indicated a predicted increase in MH landfall activity with warmer atmospheric and oceanic conditions. There are clear error bar separations between the early controls (i.e., 1860 Cntl and 1940 Cntl) and the late controls (i.e., 1990 Cntl and 2015 Cntl) for the shorter landfall droughts (e.g., 1 to 4 minimum years) and longer landfall drought (e.g., 16 + minimum years) in this figure, indicating statistically significant differences between the groups. The projected increase (decrease) in shorter (longer) MH drought events could be due to the projected increase in MH frequencies with increased anthropogenic forcing. We found that HiFLOR projected an increase in MH frequencies at the locations where simulated frequency of occurrence of MHs was in peak in the 1860 control (i.e., no track change; Figure S4).

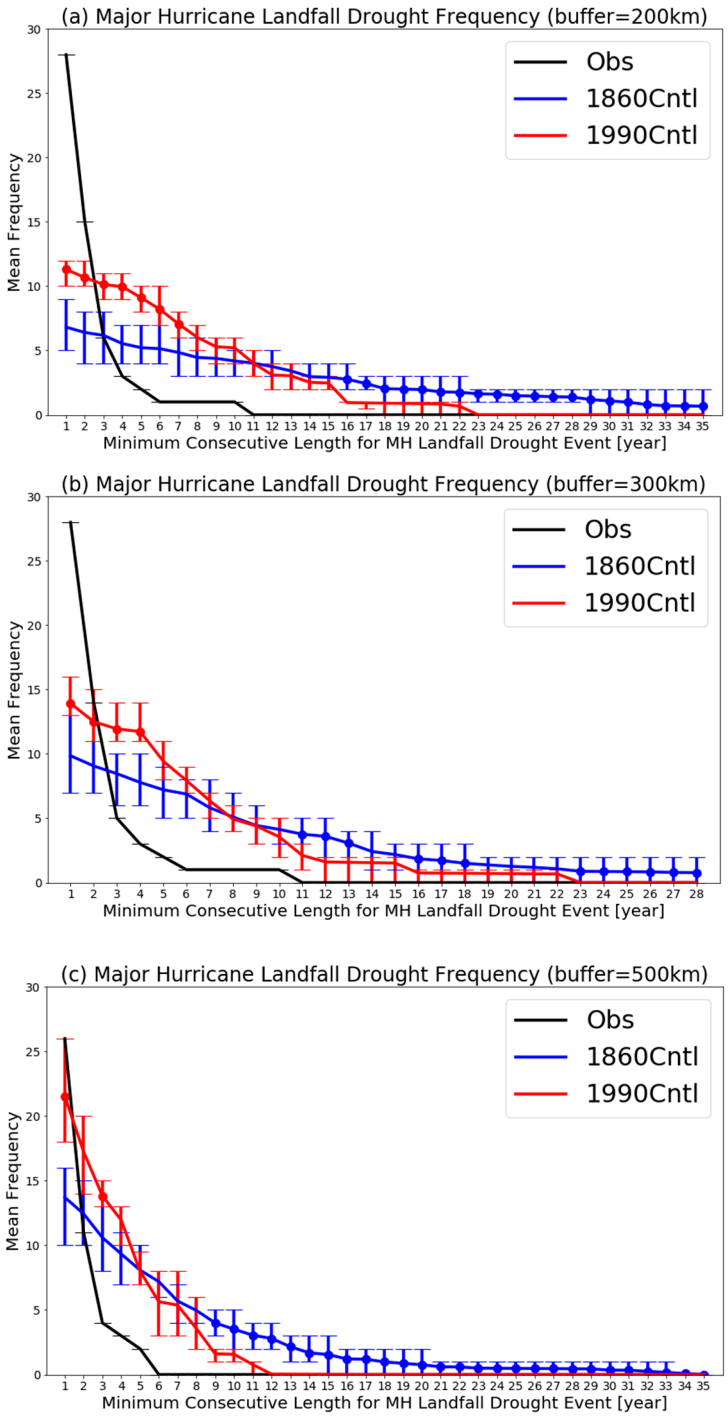

Figure 3. Mean frequencies of minimum consecutive length for MH landfall drought for (**a**) 200 km fixed-distance buffer, (**b**) 300 km buffer, and (**c**) 500 km buffer. The horizontal axis represents minimum length of MH landfall drought. For example, '20' represents MH landfall drought length longer than or equal to 20 years. The black line represents the observed MH landfall drought lengths for the United States in the 116-year period between 1900 and 2015 using six-hourly HURDDAT2 dataset. Blue (Red) line represents the 1860 (1990) control experiment. Error bars represent the 90th percentile (top bound) and 10th percentile (bottom bound) of the 116-year moving means. Red (Blue) dot indicates that simulated frequency by 1990 control is greater (smaller) statistically significantly than that by 1860 control at the 90% level.

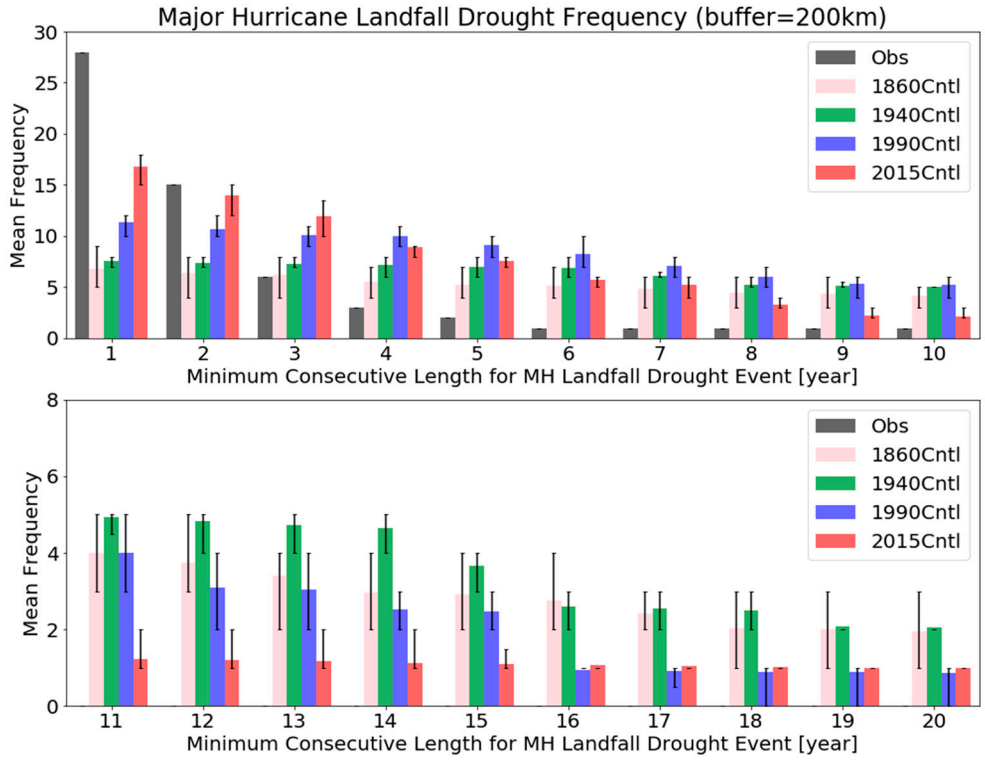

Figure 4. As in Figure 3a, but with various control simulations by the 1860 control (pink), 1940 control (green), 1990 control (blue), and 2015 control (red) along with the HURDAT2 dataset (grey).

On the other hand, compared with the six-hourly HURDAT2 frequencies of MH landfall drought, both of the 1990 and 2015 controls overestimated frequency of MH landfall droughts with minimum length longer than 3 years (Figure 4). Therefore, the HiFLOR critically overestimated the frequency of longer MH landfall drought events in the U.S., highlighting a limitation of the quantitative assessment of MH landfall drought using HiFLOR. Moreover, relatively shorter simulation lengths of 2015 control (200 years), 1990 control (300 years), and 1940 control (300 years) relative to the 1860 control (1200 years), may not be long enough to obtain statistical significance for the mutual differences in MH landfall drought frequency, especially for long-lasting MH landfall drought events, and given the fact that we could not obtain enough samples for 116-year moving means to estimate the error bars, as shown in Figures 3 and 4. A longer control simulation is necessary for an accurate estimation of MH landfall drought frequency. It is also necessary for obtaining statistically significant differences among the control simulations. However, a longer simulation is computationally expensive with a MH permitting model.

4. Summary and Discussion

We have assessed the sensitivity of landfalling TCs and landfalling MH statistics in regard to their position to the U.S. coast by creating six different buffer zones circling the U.S. East Coast. We observed six-hourly hurricane tracks in the HURDAT2 dataset in the North Atlantic Ocean from 1900 to 2015 through each buffer and calculated how many of TCs and MHs crossed the given fixed-distance buffer, in comparison to NOAA's recorded landfall events in the period 1900 to 2015. Although there were differences in MH landfall frequencies calculated with each buffer, we found that the MH landfall frequencies generated with the 200 km buffer, using the six-hourly HURDAT2 dataset were the most similar to observed recorded MH landfall frequencies. A buffer system can be utilized to correct potential error in landfall frequencies generated by six-hourly datasets, and can be utilized to analyze storm activity close to the coastline that might mimic actual landfall events.

We utilized the GFDL HiFLOR high-resolution model to examine the impact of anthropogenic warming on MH landfall drought frequency with each different buffer distance. We computed the frequency of MH landfall droughts for the 1860, 1940, 1990, and 2015 control simulations to analyze the difference in projected MH landfall frequencies with varying levels of anthropogenic forcing. We found that the later control simulations (i.e., 1990 controls and 2015 controls) generally depicted significantly higher (lower) frequencies of shorter (longer) MH landfall drought than the earlier control simulations (i.e., 1860 controls and 1940 controls). These results suggest that HiFLOR projects an increase in MH landfall frequencies with greater anthropogenic forcing. Our simulation results imply that the observed MH landfall events between 2006 and 2016 may not be relevant to the continuing increase in greenhouse gasses. The HiFLOR projections suggest that these long-lasting MH landfall droughts are likely to become rare in regard to increases in anthropogenic forcing. However, the underlying mechanisms controlling the unusually long MH landfall drought event observed between 2006 and 2016 are not clear.

Meanwhile, the HiFLOR control simulations critically underestimated MH landfall activity, as mean drought duration and frequencies were greater than the six-hourly HURDAT2 data for the period 1900 to 2015 (Figure 3). Therefore, our experiment results should not be considered quantitative because of the model biases and because the detected landfall frequencies with each buffer did not mirror observed landfall frequencies in the United States. These results merely suggest that the HiFLOR model predicts an increase in TC activity near the coastline of the United States with heightened levels of anthropogenic forcing. However, we were unable to provide quantitative changes in frequency of MH landfall drought events due to the model biases. The underestimation of MH landfall activity by HiFLOR was mainly due to the underlying cold biases in the subsurface ocean in the tropical Atlantic [28]. Fixing this bias is necessary for future accurate simulations of MH landfall activity. The use of a longer, more accurate climate simulation is also necessary to quantitatively analyze MH landfall frequencies and drought duration in the U.S. Overall, our findings have major implications for U.S. coastal communities, as MH landfall events are extremely destructive, and could result in more damage with warmer global temperatures, which is consistent with previous studies (e.g., [44]). For future analysis, we can create buffer zones according to predicted U.S. coastlines, especially as sea levels continue to rise and the U.S. coastline continues to recede [45–47].

Supplementary Materials: The following are available online at http://www.mdpi.com/2077-1312/7/5/135/s1.

Author Contributions: Conceptualization, E.L. and H.M.; Methodology, H.M.; Software, H.M.; Validation, E.L.; Formal Analysis, E.L. and H.M; Investigation, E.L. and H.M.; Resources, H.M.; Data Curation, H.M.; Writing—Original Draft Preparation, E.L.; Writing—Review & Editing, E.L. and H.M.; Visualization, H.M.; Supervision, H.M.; Project Administration, H.M.; Funding Acquisition, H.M.

Funding: This research was funded by the Cooperative Institute for Climate Science (NA14OAR4320106) and The Sandy Supplemental from the National Oceanic and Atmospheric Administration, U.S. Department of Commerce (NA14OAR4830101200).

Acknowledgments: The authors thank Gan Zhang and Heather Archambault for their suggestions and comments. The statements, findings, conclusions, and recommendations are those of the authors and do not necessarily reflect the views of the National Oceanic and Atmospheric Administration, or the U.S. Department of Commerce.

Conflicts of Interest: The authors declare no conflict of interest.

References

1. Colorado State University (CSU). Real-time North Atlantic Ocean Statistics by Storm for 2017. Available online: https://tropical.colostate.edu/media/sites/111/2017/11/2017-11.pdf (accessed on 4 May 2019).
2. Klotzbach, P.J.; Bowen, S.G.; Pielke, R.; Bell, M. Continental U.S. Hurricane Landfall Frequency and Associated Damage: Observations and Future Risks. *Bull. Am. Meteorol. Soc.* **2018**, *99*, 1359–1376. [CrossRef]
3. National Center for Environmental Information, National Oceanic and Atmospheric Administration. Billion-Dollar Weather and Climate Disasters: Table of Events. Available online: https://www.ncdc.noaa.gov/billions/events/US/1980-2018 (accessed on 4 May 2019).

4. Blake, E.S.; Zelinsky, D.A. *Hurricane Harvey. National Hurricane Center Tropical Cyclone Rep. AL092017*; 2018; 76p. Available online: https://www.nhc.noaa.gov/data/tcr/AL092017_Harvey.pdf (accessed on 4 May 2019).
5. Emanuel, K. Assessing the present and future probability of hurricane Harvey's rainfall. *Proc. Natl. Acad. Sci. USA* **2017**, *114*, 12681–12684. [CrossRef] [PubMed]
6. Miami: National Weather Servic. Costliest U.S. Tropical Cyclones Tables Updated. Available online: https://www.nhc.noaa.gov/news/UpdatedCostliest.pdf (accessed on 4 May 2019).
7. Cangialosi, J.P.; Latto, A.S.; Berg, R. *Hurricane Irma. National Hurricane Center Tropical Cyclone Rep. AL112017*; 2018; 111p. Available online: https://www.nhc.noaa.gov/data/tcr/AL112017_Irma.pdf (accessed on 4 May 2019).
8. Kishore, N.; Marqués, D.; Mahmud, A.; Kiang, M.V.; Rodriguez, I.; Fuller, A.; Ebner, P.; Sorensen, C.; Racy, F.; Lemery, J.; et al. Mortality in Puerto Rico after Hurricane Maria. *N. Engl. J. Med.* **2018**, *379*, 162–170. [CrossRef] [PubMed]
9. Hurricane Research Division, Atlantic Oceanographic and Meteorological Laboratory, National Oceanic and Atmospheric Administration. Detailed List of Continental United States Hurricane Impacts/Landfalls. Available online: http://www.aoml.noaa.gov/hrd/hurdat/UShurrs_detailed.html (accessed on 4 May 2019).
10. University of Arizona. Cycles of Atlantic Hurricanes; Global Warming and Hurricanes; Damage and Death Trends. Available online: http://www.atmo.arizona.edu/students/courselinks/fall16/atmo336s2/lectures/sec2/hurricanes3.html (accessed on 4 May 2019).
11. Hall, T.; Hereid, K. The frequency and duration of U.S. hurricane droughts. *Geophys. Res. Lett.* **2015**, *42*, 3482–3485. [CrossRef]
12. Emanuel, K.A.; Nolan, D.S. Tropical Cyclone Activity and the Climate System. In Proceedings of the 26th Conference on Hurricanes and Tropical Meteorology, Miami, FL, USA, 3–7 May 2004.
13. Vecchi, G.A.; Delworth, T.; Gudgel, R.; Kapnick, S.; Rosati, A.; Wittenberg, A.T.; Zeng, F.; Anderson, W.; Balaji, V.; Dixon, K.; et al. On the Seasonal Forecasting of Regional Tropical Cyclone Activity. *J. Clim.* **2014**, *27*, 7994–8016. [CrossRef]
14. Hall, T.; Yonekura, E. North American Tropical Cyclone Landfall and SST: A Statistical Model Study. *J. Clim.* **2013**, *26*, 8422–8439. [CrossRef]
15. Vecchi, G.A.; Msadek, R.; Anderson, W.; Chang, Y.; Delworth, T.; Dixon, K.; Zhang, S. Multiyear Predictions of North Atlantic Hurricane Frequency: Promise and Limitations. *J. Clim.* **2013**, *26*, 5337–5357. [CrossRef]
16. Wang, R.; Wu, L. Climate Changes of Atlantic Tropical Cyclone Formation Derived from Twentieth-Century Reanalysis. *J. Clim.* **2013**, *26*, 8995–9005. [CrossRef]
17. Hart, R.E.; Chavas, D.R.; Guishard, M.P. The Arbitrary Definition of the Current Atlantic Major Hurricane Landfall Drought. *Bull. Am. Meteorol. Soc.* **2016**, *97*, 713–722. [CrossRef]
18. Emanuel, K.; Sundararajan, R.; Williams, J. Hurricanes and Global Warming: Results from Downscaling IPCC AR4 Simulations. *Bull. Am. Meteorol. Soc.* **2008**, *89*, 347–368. [CrossRef]
19. Knutson, T.; McBride, J.L.; Chan, J.; Emanuel, K.; Holland, G.; Landsea, C.; Held, I.; Kossin, J.P.; Srivastava, A.K.; Sugi, M. Tropical cyclones and climate change. *Nat. Geosci.* **2010**, *3*, 157–163. [CrossRef]
20. Walsh, K.J.E.; McBride, J.L.; Klotzbach, P.J.; Balachandran, S.; Camargo, S.J.; Holland, G.; Knutson, T.R.; Kossin, J.P.; Lee, T.; Sobel, A.; et al. Tropical cyclones and climate change. *WIREs Clim. Chang.* **2016**, *7*, 65–89. [CrossRef]
21. Daloz, A.S.; Camargo, S.J.; Kossin, J.P.; Emanuel, K.; Horn, M.; Jonas, J.A.; Zhao, M. Cluster Analysis of Downscaled and Explicitly Simulated North Atlantic Tropical Cyclone Tracks. *J. Clim.* **2015**, *28*, 1333–1361. [CrossRef]
22. Klotzbach, P.J.; Landsea, C.W. Extremely Intense Hurricanes: Revisiting Webster et al. (2005) after 10 Years. *J. Clim.* **2015**, *28*, 7621–7629. [CrossRef]
23. Yoshida, K.; Sugi, M.; Mizuta, R.; Murakami, H.; Ishii, M. Future Changes in Tropical Cyclone Activity in High-Resolution Large-Ensemble Simulations. *Geophys. Res. Lett.* **2017**, *44*, 9910–9917. [CrossRef]
24. IPCC. *Climate Change 2013: The Physical Science Basis*; Cambridge University Press: Cambridge, UK, 2013; 1535p. [CrossRef]
25. Colbert, A.J.; Soden, B.J.; Vecchi, G.A.; Kirtman, B.P. The Impact of Anthropogenic Climate Change on North Atlantic Tropical Cyclone Tracks. *J. Clim.* **2013**, *26*, 4088–4095. [CrossRef]
26. Garner, A.J.; Mann, M.E.; Emanuel, K.A.; Kopp, R.E.; Lin, N.; Alley, R.B.; Pollard, D. Impact of climate change on New York City's coastal flood hazard: Increasing flood heights from the preindustrial to 2300 CE. *Proc. Natl. Acad. Sci. USA* **2017**, *114*, 11861–11866. [CrossRef]

27. Murakami, H.; Wang, B. Future change of North Atlantic tropical cyclone tracks: Projection by a 20-km-mesh global atmospheric model. *J. Clim.* **2010**, *23*, 2699–2721. [CrossRef]
28. Murakami, H.; Vecchi, G.A.; Underwood, S.; Delworth, T.L.; Wittenberg, A.T.; Anderson, W.G.; Chen, J.-H.; Gudgel, R.G.; Harris, L.; Lin, S.-J.; et al. Simulation and prediction of Category 4 and 5 hurricanes in the high-resolution GFDL HiFLOR coupled climate model. *J. Clim.* **2015**, *28*, 9058–9079. [CrossRef]
29. Bhatia, K.; Vecchi, G.; Murakami, H.; Underwood, S.; Kossin, J. Projected Response of Tropical Cyclone Intensity and Intensification in a Global Climate Model. *J. Clim.* **2018**, *31*, 8281–8303. [CrossRef]
30. Murakami, H.; Levin, E.; Delworth, T.L.; Gudgel, R.; Hsu, P.-C. Dominant effect of relative tropical Atlantic warming on major hurricane occurrence. *Science* **2018**, *362*, 794–799. [CrossRef]
31. Murakami, H.; Vecchi, G.A.; Villarini, G.; Delworth, T.L.; Gudgel, R.; Underwood, S.; Yang, X.; Zhang, W.; Lin, S. Seasonal forecasts of major hurricanes and landfalling tropical cyclones using a high-resolution GFDL coupled climate model. *J. Clim.* **2016**, *29*, 7977–7989. [CrossRef]
32. Schenkel, B.A.; Lin, N.; Chavas, D.; Vecchi, G.A.; Oppenheimer, M.; Brammer, A. Lifetime Evolution of Outer Tropical Cyclone Size and Structure as Diagnosed from Reanalysis and Climate Model Data. *J. Clim.* **2018**, *31*, 7985–8004. [CrossRef]
33. Zhang, W.; Vecchi, G.A.; Murakami, H.; Delworth, T.; Wittenberg, A.T.; Rosati, A.; Underwood, S.; Anderson, W.; Harris, L.; Gudgel, R.; et al. Improved Simulation of Tropical Cyclone Responses to ENSO in the Western North Pacific in the High-Resolution GFDL HiFLOR Coupled Climate Model. *J. Clim.* **2016**, *29*, 1391–1415. [CrossRef]
34. Landsea, C.W.; Franklin, J.L. Atlantic Hurricane Database Uncertainty and Presentation of a New Database Format. *Mon. Weather Rev.* **2013**, *141*, 3576–3592. [CrossRef]
35. Taramelli, A.; Melelli, L.; Pasqui, M.; Sorichetta, A. Estimating hurricane hazards using a GIS system. *Nat. Hazards Earth Syst. Sci.* **2008**, *8*, 839–854. [CrossRef]
36. QGIS Development Team. QGIS Geographic Information System. Open Source Geospatial Foundation Project. 2018. Available online: http://qgis.osgeo.org (accessed on 4 May 2019).
37. Chavas, D.R.; Ling, N.; Dong, W.; Lin, Y. Observed Tropical Cyclone Size Revisited. *J. Clim.* **2016**, *29*, 2923–2939. [CrossRef]
38. National Hurricane Center. Glossary of NHC Terms. Available online: https://www.nhc.noaa.gov/aboutgloss.shtml (accessed on 4 May 2019).
39. Bell, K.; Ray, P.S. North Atlantic Hurricanes 1977–99: Surface Hurricane-Force Wind Radii. *Mon. Weather Rev.* **2004**, *132*, 1167–1189. [CrossRef]
40. Delworth, T.L.; Rosati, A.; Anderson, W. Simulated climate and climate change in the GFDL CM2.5 high-resolution coupled climate model. *J. Clim.* **2012**, *25*, 2755–2781. [CrossRef]
41. Delworth, T.L.; Broccoli, A.J.; Rosati, A.; Stouffer, R.J.; Balaji, V.; Beesley, J.A.; Cooke, W.F.; Dixon, K.W.; Dunne, J.; Dunne, K.A.; et al. GFDL's CM2 global coupled climate models. Part I: Formulation and simulation characteristics. *J. Clim.* **2006**, *19*, 643–674. [CrossRef]
42. Bhatia, K.; Vecchi, G.; Kossin, J.; Knutson, T.; Murakami, H. Is Climate Change Redefining the Speed Limit of Tropical Cyclones? In Proceedings of the 33rd Conference on Hurricanes and Tropical Meteorology, Ponte, Vedra, FL, USA, 16–20 April 2018.
43. Harris, L.M.; Lin, S.-J.; Tu, C.Y. High resolution climate simulations using GFDL HiRAM with a stretched global grid. *J. Clim.* **2016**, *29*, 4293–4314. [CrossRef]
44. Emanuel, K. Global Warming Effects on U.S. Hurricane Damage. *Weather. Soc.* **2011**, *3*, 261–268. [CrossRef]
45. Bamber, J.L.; Aspinall, W.P. An expert judgement assessment of future sea level rise from the ice sheets. *Nat. Clim. Chang.* **2013**, *3*, 424–427. [CrossRef]
46. Rasmussen, D.J.; Bittermann, K.; Buchanan, M.K.; Kulp, S.; Strauss, B.H.; Kopp, R.E.; Oppenheimer, M. Extreme sea level implications of 1.5 °C, 2.0 °C, and 2.5 °C temperature stabilization targets in the 21st and 22nd centuries. *Environ. Res. Lett.* **2018**, *13*, 034040. [CrossRef]
47. Wahl, T.; Haigh, I.D.; Nicholls, R.J.; Arns, A.; Dangendorf, S.; Hinkel, J.; Slangen, A.B. Understanding extreme sea levels for broad-scale coastal impact and adaptation analysis. *Nat. Commun.* **2017**, *8*, 16075. [CrossRef]